PhotoniX

RESEARCH Open Access

Interleaved frequency comb by chip-scale acousto-optic phase modulation at polydimethylsiloxane for higher-resolution direct plasmonic comb spectroscopy

San Kim[1], Tae-In Jeong[1], Robert A. Taylor[2], Kwangseuk Kyhm[1,4], Young-Jin Kim[3*] and Seungchul Kim[1,4*]

*Correspondence: yj.kim@kaist.ac.kr; s.kim@pusan.ac.kr

[1] Department of Cogno-Mechatronics Engineering, College of Nanoscience and Nanotechnology, Pusan National University, 2 Busandaehak-Ro 63Beon-Gil, Busan 46241, South Korea
[2] Department of Physics, Clarendon Laboratory, University of Oxford, Oxford OX1 3PU, UK
[3] Department of Mechanical Engineering, Korea Advanced Institute of Science and Technology (KAIST), 291 Daehak-Ro, Yuseong-Gu, Daejeon 34141, South Korea
[4] Department of Optics & Mechatronics Engineering, College of Nanoscience and Nanotechnology, Pusan National University, 2 Busandaehak-Ro 63Beon-Gil, Busan 46241, South Korea

Abstract

High-resolution spectroscopy unveils the fundamental physics of quantum states, molecular dynamics, and energy transfers. Ideally, a higher spectral resolution over a broader bandwidth is the prerequisite, but traditional spectroscopic techniques can only partially fulfill this requirement even with a bulky system. Here we report that a multi-frequency acousto-optic phase modulation at a chip-scale of soft polydimethylsiloxane can readily support a 200-times higher 0.5-MHz spectral resolution for the frequency-comb-based spectroscopy, while co-located plasmonic nanostructures mediate the strong light-matter interaction. These results suggest the potential of polydimethylsiloxane acousto-optic phase modulation for cost-effective, compact, multifunctional chip-scale tools in diverse applications such as quantum spectroscopy, high-finesse cavity analysis, and surface plasmonic spectroscopy.

Keywords: Optical spectroscopy, Chip-scale acousto-optic phase modulation, Polydimethylsiloxane, Frequency comb, Plasmonics

Introduction

High-resolution optical spectroscopy has been a vital tool for unveiling the new physics of quantum phenomena, including the analysis of complex chemical elements [1, 2], the observation of molecular quantum motion [3–5], and the study of single spin states of atoms [6–8]. The spectral proximity of optically excited spins or vibrational modes linked to intricate molecular bonds poses a challenge for distinguishing them via traditional spectrometers or monochromators based on diffraction gratings. These necessitate the use of novel spectroscopic methods that offer high spectral resolution in a simple and compact manner. Fourier transform spectroscopy has long been used for high-resolution spectroscopy [9], but its resolution is limited to about 30 MHz, and the long mechanical scanning of the interferometer arm requires high-precision control, not suitable for harsh environments or small-scale integrated devices. Frequency comb (FC) spectroscopy [10] provides a promising alternative for high-resolution spectral measurements, as it allows for scalability and adaptability to chip-scale micro-resonators [11, 12],

optical communications [13] or photonic integrated circuits [14]. FC generates a large number of optical frequencies that are highly coherent in the frequency domain [15], providing superior performance in the spectral analysis of gas atoms and molecular fingerprinting studies [1–3]. Furthermore, the FC, being coupled to atomic clock frequencies could serve as a cornerstone for mapping the internal atomic energy structure and atomic dynamics for the regulation of fundamental constants [6–8].

Direct frequency comb spectroscopy (DFCS) [16–18] is one of the representative methods for high-resolution FC spectroscopy, owing to its simplicity and robustness. It involves the interaction of an FC with target atoms and molecules to produce absorption features that provide information about specific electronic transition lines. The spectral resolution of DFCS is constrained by the frequency spacing between two neighboring optical modes, usually spanning from tens of MHz to a few GHz, attributable to the repetition frequency of the mode-locked laser pulse [15]. Thus, extending the cavity length of a mode-locked laser can reduce a repetition frequency to sub-MHz level for high-resolution DFCS. However, this approach requires much effort in laser stabilization that limits practical applications. Recently, a pulse-picking technique utilizing an acousto-optic modulator (AOM) has been demonstrated to reduce the repetition frequency to the sub-MHz level. This method incorporates pulse amplification to generate sufficient powered mode-locked laser pulses [19].

Meanwhile, the spectral resolution of DFCS can be improved by employing phase modulation techniques without optical amplifier, which create interleaved combs between optical modes [20]. This technique involves actively modulating the refractive index of the medium through which light is transmitted. Generally, the phase modulation in a medium can be quantified by the phase modulation index β, describing the degree of phase change due to the modulation angular frequency [21]. A high phase modulation index corresponds to the generation of many interleaved comb modes with a quasi-flat power distribution. These interleaved comb modes through phase modulation techniques enhance the spectral resolution of DFCS, contingent upon the frequency of the phase modulation.

Conventional optical phase modulation techniques have primarily used high second-order nonlinearity materials like $LiNbO_3$ to modulate the refractive index of the medium in an electrical manner [22–24]. $LiNbO_3$ offers high electro-optic coefficients, enabling efficient phase modulation even at low voltages. Additionally, they provide high linearity in phase modulation, making them well-suited for GHz-range optical communication with high precision. However, $LiNbO_3$-based phase modulators have several demerits, including limited fabrication forms with costs, which prevent them from realizing the full potential of the material. While various on-chip optical modulators have been reported to date [22–27], they generally have required sophisticated fabrication processes. Acoustic waves can be used as an alternative way to realize phase modulation through modulating the refractive index of the non-conducting medium [21, 28]. As the acoustic waves propagate through the medium, the density of the medium changes in synchrony with the modulation frequency, which in turn can modulate the phase of light traveling through the medium. However, conventional acoustic wave-based phase modulators continue to use bulky and solid materials such as SiO_2 and TeO_2 [28], which fail to achieve strong phase modulation effects with moderately powered piezoelectric

transducers. Recently, the use of acoustic waves with unconventional mediums like air has demonstrated new possibilities to advance novel acoustic optical manipulation [29]. Meanwhile, recent interest has focused on the study soft material-based devices to achieve multifunctional optoelectronic effects in a flexible form [30]. This has been particularly exploited in the field of flexible electronics, where the ability to bend and stretch electronic devices provides a broad spectrum of application benefits.

Polydimethylsiloxane (PDMS) is an amorphous silicon elastomer composed of Si–O, Si–C, and C–H covalent bonds, consisting of $[Si(CH_3)_2O]_n$ monomeric units that repeat approximately 250 to 300 times to form polymer chains. The polymer chains react with an injected curing agent to form chemical cross-links between the terminal or side groups of the chains. A high density of cross-links strengthens the inter-chain bonds, resulting in increased stiffness while reducing both flexibility and viscoelasticity. In contrast, when the crosslinking density is low, the inter-chain bonds are weakened, and loose intermolecular interactions, primarily governed by van der Waals forces, become predominant. This leads to enhanced flexibility and viscoelasticity. By controlling the crosslinking density, PDMS can achieve a low elastic modulus, which results in a slower acoustic wave propagation speed compared to crystalline media such as SiO_2 or TeO_2. The low elastic modulus allows PDMS to deform easily under external stress, inducing significant molecular structural changes in response to acoustic waves. This, in turn, produces a high elasto-optic coefficient. Additionally, PDMS exhibits high optical transmittance across a broad spectral range from visible to mid-infrared due to its amorphous structure with minimal internal defects, consisting of polymer chains formed by repetitive Si–O and C-H bonds, which have narrow absorption spectra in the infrared region caused by vibrational–rotational modes [31]. The low acoustic velocity, high elasto-optic coefficient, and broadband optical transmittance make PDMS an exceptionally efficient material for acoustic-based optical modulation. Moreover, PDMS enables easy replication of intricate structures through simple mold casting and exhibits strong substrate adhesion, allowing seamless integration into various device architectures such as plasmonic nanostructures [32]. Remarkably, despite the high acousto-optic modulation efficiency of soft PDMS, driven by its low acoustic wave velocity and high elasto-optic coefficient, and its compatibility with hybrid optoelectronic devices, the application of soft PDMS for acousto-optic modulation has not been extensively explored.

In this study, we introduce chip-scale PDMS as a novel soft material for acousto-optic phase modulation of a FC, enabling the generation of a highly precise comb source with 0.5 MHz mode spacing, achieving a spectral resolution 200 times greater than that of conventional FCs. Additionally, we demonstrate a fourfold increase in the phase modulation index at modulation frequencies ranging from 0.2 to 2 MHz, while maintaining nearly consistent performance under 8% compressive strain in PDMS. Interestingly, the phase modulation intensity is not affected by the direction of the induced acoustic wave, suggesting that the phase modulation performance can be achieved by using dual or multiple phase modulation in various directions; thereby, more than 36 interleaved comb modes could potentially be generated around each existing optical mode, fully populating the 100 MHz span while maintaining a signal-to-noise ratio (SNR) of at least 10 dBm. Our results confirm that PDMS, possessing high optical transparency, is capable of providing phase-modulated FCs without noticeable degradation in its frequency

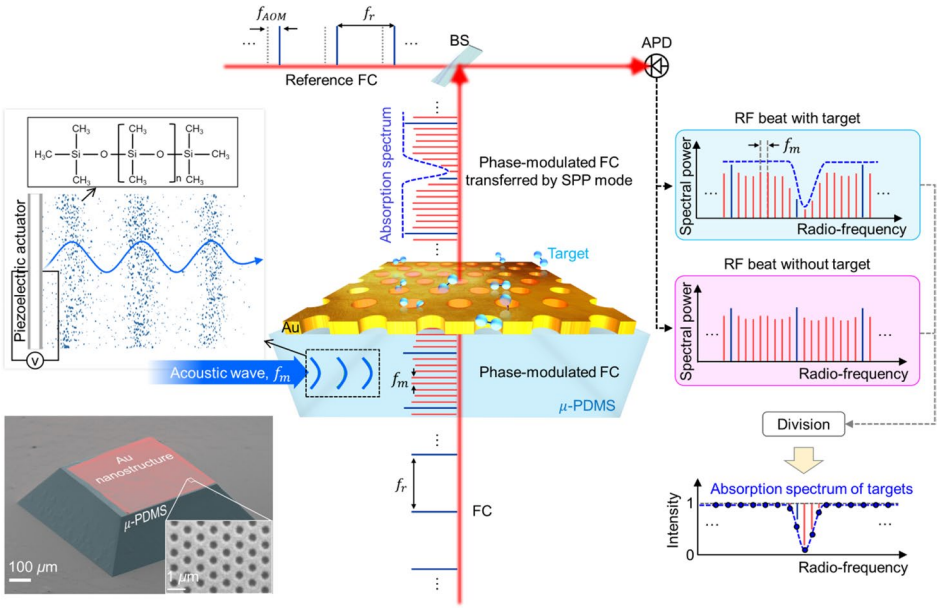

Fig. 1 A schematic illustration of the microscale-PDMS phase modulator incorporating plasmonic nanostructures and the process of direct frequency comb spectroscopy measuring the target absorption spectrum. When the FC passes through the μ-PDMS, it undergoes acousto-optic phase modulation by the acoustic wave frequency of f_m. This process generates new interleaved combs with a frequency spacing of f_m. The phase-modulated FC is then transformed to the plasmonic mode, allowing more efficient interaction with the target materials on the Au surface. This plasmonic FC is subsequently transformed back into the photonic FC and combined with a reference FC whose frequency is shifted by f_{AOM} (40 MHz), to produce a RF beat frequency. These RF beat spectrum possess the absorption spectral features of the target gas (right panel). The bottom left panel shows the SEM image of plasmonic nanostructures integrated μ-PDMS. SPP: surface plasmon polariton, BS: beam splitter, APD: avalanche photodetector

characteristics. This exceptional performance allows PDMS to be integrated seamlessly with plasmonic nanostructures, whose feasibility was confirmed by a high-resolution spectroscopic analysis of a Fabry-Pérot interferometer (FPI) proving a sub-MHz resolution with an absolute position tracing capability referenced to the FC. This demonstrates the potential use of our PDMS-based acousto-optic phase modulation in a multifunctional compact spectroscopic tool for the real-time monitoring of high-finesse single-crystal Si cavities [33], and plasmonic phase spectroscopy [34] including high-resolution DFCS.

Results

Acousto-optic phase modulation of FC in PDMS

Figure 1 depicts the process involved in the generation of a phase-modulated FC using plasmonic nanostructure integrated microscale-PDMS (μ-PDMS), and the subsequent DFCS measurements. An FC comprises numerous precisely defined optical frequencies and any given optical frequency within the FC can serve as a reference optical frequency for the phase modulation, denoted as

$$f_0(k) = f_{ceo} + k \cdot f_r \tag{1}$$

where f_{ceo} indicates the carrier-envelope offset frequency, and $k \cdot f_{\mathrm{r}}$ represents the mode number multiplied by the repetition frequency [15]. The FC's phase is modulated by modulating the refractive index of the μ-PDMS sinusoidally by applying an acoustic frequency provided by a piezoelectric actuator. The phase-modulated electric-field of the k_{th} optical mode can be expressed as [35]

$$E_{\mathrm{PM}}(t,k) = E_0(k) \sum_{a=-\infty}^{\infty} J_a(\beta) \cos\left[2\pi \left(f_0(k) + a \cdot f_{\mathrm{m}}\right) t\right] \tag{2}$$

where $E_0(k)$ represents the amplitude of the electric-field for the k_{th} optical mode in the FC, $J_a(\beta)$ refers to the Bessel function corresponding to β, f_{m} signifies the acoustic modulation frequency, and a is an integer. Thus, the phase-modulated electric-field produces new optical modes, which are separated from each $f_0(k)$ at discrete uniform intervals of f_{m}. These new optical modes can improve the resolution of the DFCS and be tuned by adjusting the acoustic modulation frequency. However, when β is small, the power of these new interleaved comb modes decreases rapidly as their frequencies diverge from $f_0(k)$ because, with an increase in a, the power of the a_{th} optical mode is lowered by higher-order Bessel functions $J_a(\beta)$. As a result, this creates a noticeable measurement dead zone, centrally situated between the two neighboring optical modes $f_0(k)$ and $f_0(k+1)$. Thus, it is crucial to increase the value of β to generate wider interleaved combs between two neighboring optical modes $f_0(k)$ and $f_0(k+1)$.

Theoretically, β is proportional to the refractive index change of the material Δn induced by an acoustic wave (see Supplementary Note 1) [21]. The Δn of any material is characterized by the material parameter M, which is proportional to the square of Δn and quantifies the effectiveness of the acoustic wave in altering the refractive index. The longitudinal velocity of the acoustic wave in a medium is correlated with M, which, in turn, is inversely proportional to the cube of the acoustic wave velocity and exerts a dominant influence on the value of Δn. Thus, a lower acoustic wave velocity leads to a higher value of M, resulting in a larger change of refractive index and, consequently, a higher value of β. This fundamental relationship highlights the pivotal role of the acoustic wave velocity in enabling efficient phase modulation and provides a crucial design parameter for wider interleaved comb spectroscopy. Notably, the acoustic wave velocity in a PDMS is known to be approximately 1000 m s^{-1} [36], a value significantly lower than that of materials employed in conventional AOMs, such as SiO_2 (~ 6000 m s^{-1}) [37] or dense flint glass (~ 3630 m s^{-1}) [38].

The use of PDMS increases the value of Δn greatly for acoustic wave-induced phase modulation in a medium. As a result, PDMS, as a phase modulation medium, can provide more interleaved combs thanks to its intriguing material properties, which effectively increase the value of β. In our scheme, plasmonic nanostructures were additionally embedded on a μ-PDMS, making them suitable for both DFCS and plasmonic comb spectroscopy [34], as illustrated in the scanning electron microscope (SEM) image of Fig. 1. The plasmonic resonant fields can force gaseous molecules toward the metal surface because of thermophoresis-assisted optical confinement effects [39, 40]. This approach allows for the realization of not only efficient but also compact DFCS of a gas, as the plasmonic effect reinforces the light-matter interaction without using a bulk external cavity [41]. The incident phase-modulated FC at the photonic mode is converted to

the plasmonic mode by coupling with free electrons present at the interface between the plasmonic nanostructure and the μ-PDMS. A plasmonic structure composed of a subwavelength Au nanohole array, similar in design to the structure studied in plasmonic phase spectroscopy [34] was applied, and optimized to resonate around the central frequency of the FC (see Supplementary Fig. S1 for details). The FC at the plasmonic mode passes through the subwavelength nanoholes in the form of a surface plasmon polariton (SPP) and is coherently converted to photons, so called extraordinary optical transmission. The FC transferred by the SPP mode maintains its own optical properties such as phase noise, frequency stability, and linewidth [42]. This FC, which carries the target absorption spectrum, experiences interference with the referenced FC, whose frequency is shifted by f_{AOM}, and generates a heterodyne beat in the radio-frequency (RF) domain. This RF beat provides an absorption spectrum in the optical frequency regime using RF instruments by down-converting the optical frequencies. The absorption spectrum from the target is extracted by comparing the two RF beats, with and without the target. In this process, the phase-modulated FC offers more measurement points, allowing a more accurate analysis of the target material's absorption spectrum.

Acousto-optic phase modulation characterization of PDMS

Figure 2 presents a comprehensive analysis of the phase modulation characteristics between PDMS and the conventional phase modulation material, SiO_2. The precision and bandwidth of the phase modulation frequencies are evaluated using an RF beat measurement with reference to the FC, which reflects the characteristics of the phase-modulated FC (see Supplementary Fig. S2a for a detailed measurement method). The reference FC is frequency-shifted by 40 MHz (f_{AOM}) using a commercial acousto-optical frequency shifter (AOM- 402 AF3, IntraAction corp.) to measure RF beat frequencies without low frequency noise. The RF beat spectrum shows that the PDMS phase modulator generates a modulation bandwidth of 4 MHz at a modulation frequency of 0.2 MHz, which is 1.6 times wider than the case for SiO_2 under the same experimental conditions encompassing the geometric properties of the medium, incident light power, and SNR of the reference optical modes (Fig. 2b) (see Supplementary Note 3 for details on the monitoring setup). This corresponds to a high β of 10 radians, converted from the phase modulation bandwidth based on Carson's rule, while the β in SiO_2 is about 5 (see Supplementary Note 2 for detailed calculations). The PDMS phase modulator exhibited a notably higher β compared to SiO_2, with values ranging from a minimum of 4 radians to a maximum of 11 radians. The phase modulation value resembling a kink at 600 kHz in both materials can be attributed to the characteristics of the piezoelectric component resonating at 600 kHz. Additionally, the beam profile of the FC, phase-modulated through the PDMS phase modulator, showed no noticeable changes (see Supplementary Fig. S3).

A distinctive feature of the PDMS phase modulator is its capability to induce a consistent phase modulation power irrespective of the spatial relationship between the acoustic wave and the optical paths. The equivalent values of β were measured at relative incident angle differences of 0, 45, and 90 degrees between the acoustic wave and the injected FC, as shown in Fig. 2c. Hence, the PDMS phase modulator presents a significant advantage for innovative optoelectronic design, facilitating versatility in structural form

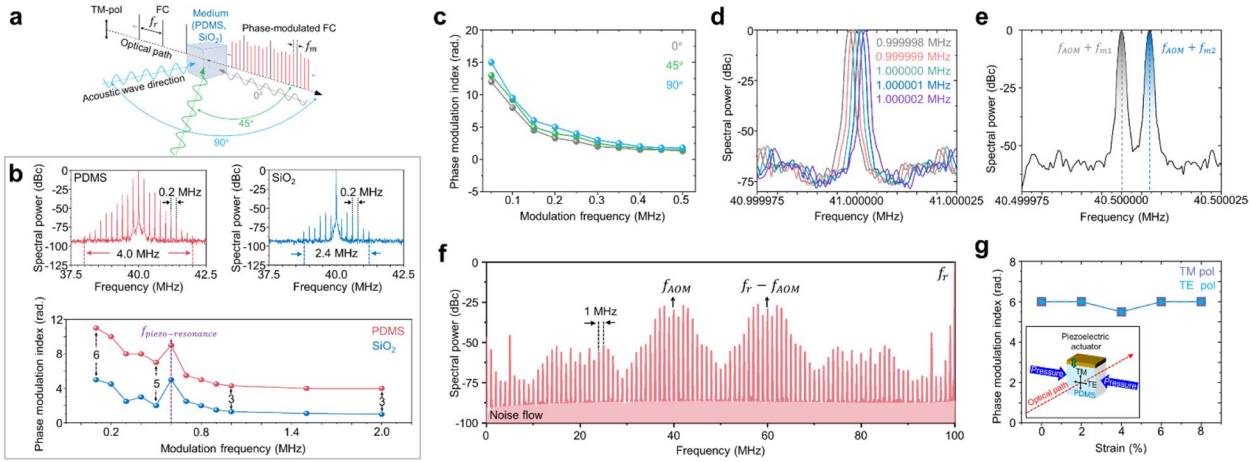

Fig. 2 Acousto-optic phase modulation characteristics of the PDMS. **a** An experimental apparatus to characterize acousto-optic phase modulation of the PDMS and SiO_2. **b** The RF beat spectra of the phase-modulated FCs from PDMS (red) and SiO_2 (blue) were measured by an RF spectrum analyzer (upper panel). The phase modulation index (β) is calculated from the RF beat spectrum at each acoustic modulation frequency (lower panel). **c** A plot of the phase modulation index for three different incident angles of the acoustic wave 0° (gray), 45° (green), and 90° (sky). **d** A measurement of the first-order phase-modulated optical mode while shifting the acoustic wave frequency in increments of 1 Hz. **e** A measurement of the first-order phase-modulated optical mode with dual acoustic waves whose frequencies are 0.500000 MHz (f_{m1}) and 0.500007 MHz (f_{m2}) at different incident angles, simultaneously. **f** RF beat speactrum of dual-phase-modulated FC with a 100 MHz span. The modulation frequencies are 1 MHz and 5 MHz. RBW and VBW are 5.1 kHz. **g** A measurement of the phase modulation index of PDMS under compressive strain ranging from 0 to 8%. The incident light polarization was set to transverse magnetic-field (TM) and transverse electric-field (TE) directions, respectively

unconstrained by the incident light's orientation. This attribute distinctly sets it apart from the design characteristics of traditional phase modulators. To assess the frequency tunability of the PDMS phase modulator, the beat frequency ($f_{AOM} + f_m$) of the first-order phase-modulated optical mode was systematically monitored with an increasing modulation frequency of 1 Hz. Note that the resolution bandwidth (RBW) and video bandwidth (VBW) of our RF spectrum analyzer (E4440 A, Agilent) is limited to 1 Hz. The phase-modulated FC showed a corresponding frequency shift with each 1 Hz increment in the modulation frequency, while preserving its spectral power and bandwidth (Fig. 2d).

Interleaved comb modes generated by phase modulation intrinsically exhibit a gradual power reduction as they locate away from the reference frequency, leading to degraded SNR, reduced sensitivity, and limited spectral bandwidth in DFCS. To overcome this power reduction issue in phase modulation, we devised a dual-phase modulation scheme by applying two individual acoustic waves with different frequencies to the PDMS. This approach enables the formation of interleaved comb modes with higher power over a broad frequency range.

PDMS phase modulator can consistently induce multiple-phase modulation in any direction, allowing for the implementation of dual-phase modulation using two piezoelectric elements, as demonstrated in Fig. 2e. There is no degradation and distortion of modulated frequencies due to the interference between the two different acoustic waves during modulation. Figure 2f presents the RF beat spectrum of the dual-phase-modulated FC, implemented with modulation frequencies of 1 MHz and 5 MHz. As a result, interleaved comb modes were uniformly distributed at 1 MHz spacingacross the entire 100 MHz spectral bandwidth, achieving a SNR of at least 10 dBm. Furthermore, by adjusting the frequency value of two acoustic waves applied to the PDMS, the dual-phase modulation enabled flexible tuning of the frequency spacing (see Supplementary Fig. S4 for details). A notable characteristic of PDMS is its ability to maintain an almost uniform value of β in the presence of mechanical compression up to compressive strain of 8%, as shown in Fig. 2f (see Supplementary Fig. S5 for detail experimental method). This characteristic underpins its potential for the development of active devices that remain robust against perturbations from external environmental factors.

DFCS of an FPI using a chip-scale μ-PDMS phase modulator

While basic optical studies using PDMS, such as refractive index measurement and optical transmittance, have been undertaken for applications in micro-lenses [43] and optofluidic devices [44], the exploration of optical phase noise analysis in PDMS remains absent, which is a crucial step for ultra-precision FC spectroscopy. PDMS, a silicon-based polymeric material, may have a non-uniform refractive index distribution due to variations in density or chemical properties over its entire area during the curing process from its liquid state. This non-uniformity can introduce irregular spatial phase noise in FCs as they propagate through the PDMS phase modulator. Consequently, elevated phase noise levels lead to linewidth broadening of phase-modulated FCs. Figure 3a shows an experimental schematic for evaluating the linewidth of phase-modulated FCs using an external cavity diode laser (ECDL) with a narrow linewidth of about 50 kHz (see Supplementary Fig. S2b for detail set-up). The FC with a beam diameter of 2 mm

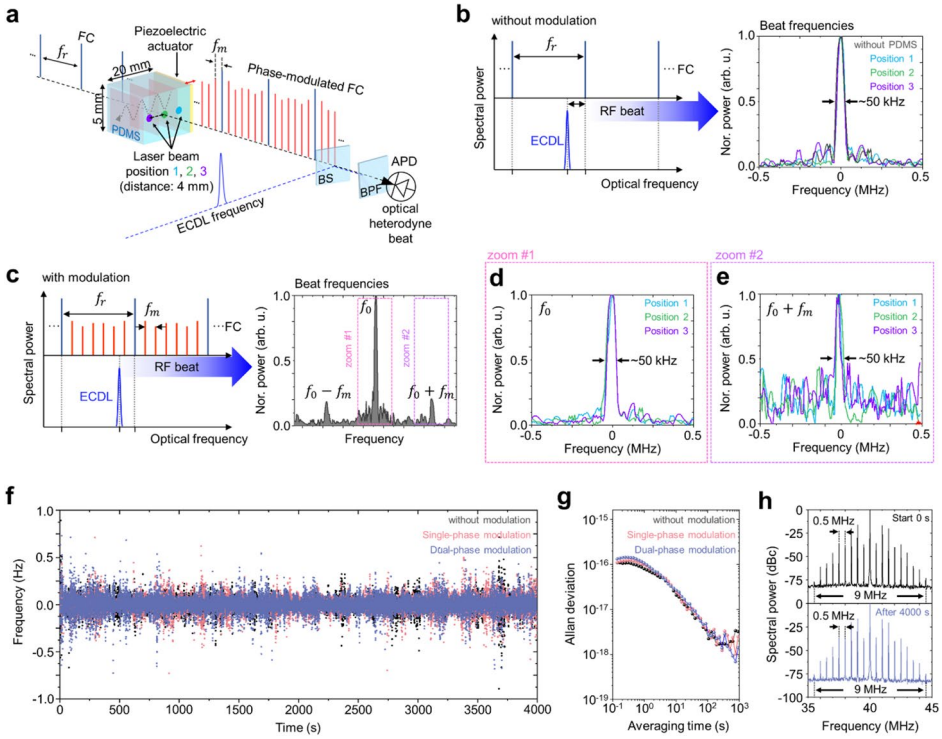

Fig. 3 Phase and frequency stability of phase-modulated frequency combs using PDMS. **a** An experimental setup for characterizing acousto-optic phase modulation at three distinct positions in PDMS, including the generation of RF beat frequencies through the interference between the phase-modulated FC and the ECDL to assess the phase-modulated FC's linewidth. An optical bandpass filter with a 1.2 nm bandwidth centered at 780 nm was used for RF beat frequency measurement. **b** Linewidth measurements of RF beat frequencies from an unmodulated FC. **c** RF beat frequencies of an original FC subjected to a phase modulation frequency of 1 MHz. **d**, **e** RF beat frequencies of the original FC (**d**) and the derived phase-modulated optical mode (**e**), which centered in a first-order phase-modulated optical mode. In all cases, a full width at half maximum linewidth of 50 kHz was observed, with no noticeable degradation. **f** Time trace of the RF beat frequency measured for 4,000 s for single-phase modulation (light coral), dual-phase modulation (glaucous), and without modulation (black). **g** Allan deviation of frequency stability over time for single-phase modulation (light coral), dual-phase modulation (glaucous), and without modulation (black). **h** RF beat spectra of the dual-phase-modulated FCs when 1.0 MHz and 1.5 MHz acoustic waves are applied to PDMS, measured immediately (0 s, black) and after 4,000 s (glaucous)

undergoes phase modulation while passing through the hexahedral PDMS with dimensions of 20 mm $\times$ 5 mm $\times$ 20 mm. A sinusoidal acoustic wave is applied through a piezoelectric actuator, oriented perpendicular to the optical path. This modulated signal is then superimposed onto a continuous-emission ECDL operating at the same center wavelength of 780 nm that provides the reference linewidth of optical frequency. The resulting optical heterodyne RF beat is measured in the same manner using an RF spectrum analyzer for phase noise analysis. In this analysis, linewidth measurements were conducted at three distinct positions on the PDMS: the center, and 4 mm to both the left and right of the center, as indicated in Fig. 3a. Figure 3b presents the linewidth measurements of the original FC at three distinct positions on the PDMS, without the influence of an acoustic wave (color-coded in sky, green, and violet), and features a measurement in the absence of a PDMS medium (shown in dark gray). Across all scenarios, the full width at half maximum (FWHM) of the RF beat frequencies was consistently around 50

kHz, aligning with the original linewidth of the ECDL. Remarkably, the application of an acoustic wave frequency of 1 MHz to the PDMS, as shown in Fig. 3c, did not cause to any significant broadening of the original FC linewidth at any of the measured positions, as demonstrated in Fig. 3d. This evidence strongly suggests that PDMS does not contribute substantial phase noise to the original FC during the phase modulation process. Importantly, the linewidth of the beat frequency derived from the phase-modulated FC remained stable, as illustrated in Fig. 3e. The beat frequencies from the phase-modulated FC, measured at three disparate positions, showed a consistent phase noise. This conclusively indicates that the phase modulation properties of PDMS are not significantly influenced by the conditions of optical alignment.

To evaluate the long-term stability of the PDMS phase modulator, we measured the frequency stability and phase modulation efficiency. The frequency stability was analyzed by monitoring the RF beat frequency at 40 MHz for 4,000 s, using heterodyne interferometer (see Supplementary Fig. S2a for the detail experimental setup). The standard deviation of RF beat frequency of the original FC was approximately 63.5 mHz, while those of the single-phase and dual-phase-modulated FCs were 69.5 mHz and 70.2 mHz, respectively (Fig. 3f). In addition, the frequency stability of the RF beat frequency was maintained at approximately 2.48×10^{-18} over an averaging time of 1,000 s for all cases, indicating no noticeable degradation in the frequency stability during phase modulation (Fig. 3g). Figure 3h presents the RF beat spectrum of the dual-phase-modulated FC measured immediately (black) and after 4,000 s (glaucous). There is no significant change in the interleaved comb after 4,000 s. These results support that the PDMS phase modulator can be suitable for long-term operation.

Figure 4a illustrates a sophisticated μ-PDMS phase modulator platform incorporating plasmonic nanostructures. The μ-PDMS phase modulator was crafted on a microscale truncated pyramid mold to easily tear off the 100 nm thick nanohole structured Au film from the Si_3N_4 substrate (see Supplementary Fig. S6a for details). The designated plasmonic nanostructure comprises hexagonally arranged nanoholes with a diameter of 400 nm and a pitch of 800 nm (see Supplementary Fig. S1a for details). Although the thin plasmonic Au film is inherently sensitive to mechanical stress, the SEM image revealed that it remained undamaged after long-term exposure to an acoustic wave through the μ-PDMS substrate (see Supplementary Fig. S1b). Intriguingly, the strength of the phase modulation remained consistent at a modulation frequency of 4 MHz, even after the integration of the plasmonic Au film (Fig. 4b). Even when the PDMS was integrated with the thicker Au/Si_3N_4 film, there was no observed deterioration in phase modulation performance, nor any damage to the films (see Supplementary Fig. S6b, c). This supports the assertion that equivalent refractive index modulations can be achieved when the PDMS is anchored to a solid substrate such as Si_3N_4, making it applicable in various silicon photonics applications. Furthermore, the modulation precision and linewidth remained undisturbed in the phase modulator integrated with the plasmonic nanostructure (Fig. 4c, d).

To evaluate the DFCS performance of the phase-modulated FC, we generated widely distributed interleaved comb with sub-MHz mode spacing via μ-PDMS phase modulator, we strategically applied modulation frequencies of 1.0 MHz and 4.5 MHz to the PDMS. This approach was meticulously designed to ensure that the interleaved

comb modes, positioned at sub-MHz intervals, exhibit a uniform power distribution (see Supplementary Fig. S7 for details).

When 1.0 MHz and 4.5 MHz acoustic waves are individually applied to the PDMS, 8 interleaved comb modes are generated at 1.0 MHz excitation, while 4 interleaved comb modes appeared at 4.5 MHz excitation (see Supplementary Fig. S7a, b). In contrast, when both acoustic waves are simultaneously applied for dual-phase modulation, more than 36 interleaved comb modes were generated with 0.5 MHz spacing, spanning a range of over 20 MHz (see Supplementary Fig. S7c). The interleaved comb modes generated via dual-phase modulation result from the combination of both modulation frequencies. Initially, modes appeared at 1.0 MHz and 4.5 MHz spacing relative to the central frequency, directly corresponding to the applied acoustic frequencies, $f_{1.0}$ and $f_{4.5}$ (blue circles, magenta stars in Supplementary Fig. S7c). Additional modes arise from the beating between the two induced acoustic frequencies, forming broad spectral bandwidth of approximately 100 MHz with 0.5 MHz spacing. (see Supplementary Fig. S7d).

Employing μ-PDMS-based DFCS, we measured the spectral transmission bandwidth of the high-finesse tunable FPI (SA30 - 73, Thorlabs), which exhibits a spectral resolution of the 1 MHz (Fig. 4f). The phase-modulated FCs transmitted through the FPI are transduced into RF frequencies using the same optical heterodyne beating with a reference FC. The transmittance for individual optical modes was characterized by comparing the intensities of each RF FC acquired in the presence and absence of the FPI. In our experiments, we distinctly captured the transmission spectrum of the FPI below 1 MHz bandwidth using our phase-modulated FC, a capability not achievable with the original FC's 100 MHz frequency spacing. Additionally, our system facilitated the detection of shifts in the FPI's transmission spectrum through precise tuning of its cavity length (Fig. 4g).

Discussion

As the proportion of PDMS base decreases in PDMS synthesis, the concentration of the curing agent correspondingly increases, leading to a higher degree of polymer cross-linking. This occurs because the curing agent facilitates polymer bonding, driving the material toward a solid state. Consequently, a lower ratio of PDMS base results in increased hardness and mass density, forming a stiffer structure with greater mechanical resistance but reduced flexibility. In contrast, as the PDMS base ratio increases, the extent of polymer cross-linking decreases, yielding a softer, less dense PDMS structure with diminished mechanical strength. Thus, the increase in the PDMS base ratio leads to a rise in elasticity. According to the equation provided in Supplementary Note 1, as the PDMS base content increases, the density of the synthesized PDMS decreases, which slows the propagation acoustic wave velocity v_s. Simultaneously, the increased elasticity enhances the elasto-optic coefficient p. These parameters theoretically increase the value of M; in other words, the Δn induced by acoustic waves increases significantly, thereby effectively inducing acoustic phase modulation. In summary, increasing the PDMS base ratio enhances acousto-optic phase modulation; however, this comes at the cost of reduced structural stability and form retention of the synthesized PDMS material. As a result, the PDMS base ratio cannot be increased indefinitely without compromising the material's practical applicability.

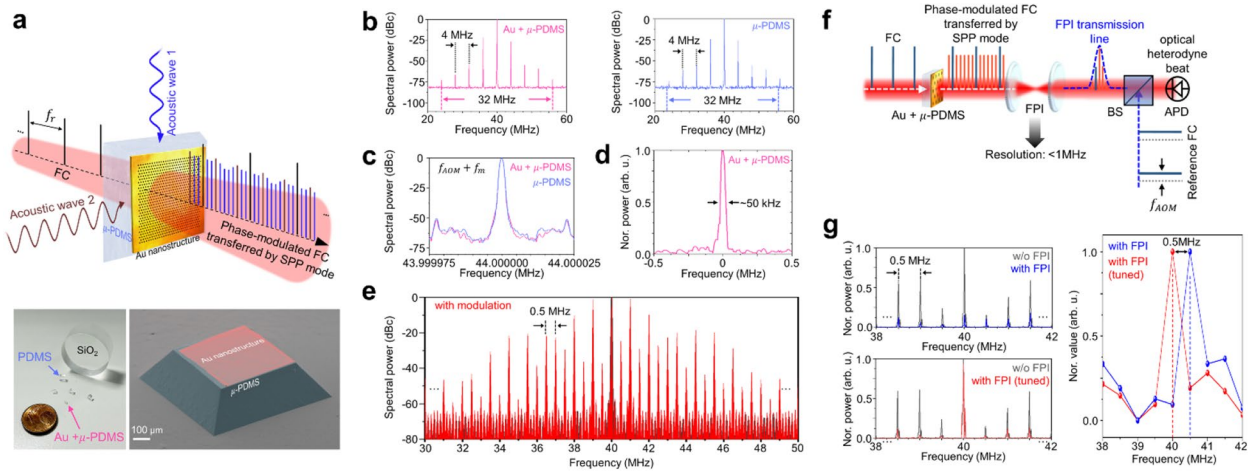

Fig. 4 Direct frequency comb spectroscopy of Fabry-Pérot interferometer using a μ-PDMS incorporating plasmonic nanostructure. **a** A schematic sketch of the a phase-modulated FC in μ-PDMS with dual phase modulation (upper panel). The photographic and the SEM image of Au plasmonic nanostructure integrated μ-PDMS used in these experiments (lower panel). **b** Comparative analysis of phase-modulated FCs with Au nanostructure integrated onto PDMS (left panel) versus without Au nanostructure (right panel). The modulation frequency was set at 4 MHz for both cases, each achieving an identical modulation bandwidth of 32 MHz, spaced at 4 MHz intervals. **c** Modulation precision of the first-order phase-modulated optical mode with Au nanostructure integrated onto PDMS (pink) versus without Au nanostructure (blue). **d** Linewidth evaluation of the original FC with Au nanostructure integrated onto PDMS. **e** An RF beat spectrum generated by the phase-modulated FC using dual-phase modulation frequencies of 1.0 MHz and 4.5 MHz (red). **f** A schematic diagram for the DFCS measurement of a FPI using the phase-modulated FC depicted in Fig. 4e. The FPI has a spectral resolution below 1 MHz. **g** An RF spectrum of DFCS after passing the FPI in the initional condition (upper left panel) after tuning (lower left panel). The transmission spectrum of the FPI is represented by dividing the DFCS data obtained with the FPI by the reference DFCS data measured without the FPI (right panel)

In this study, we harnessed the properties of PDMS to achieve higher-resolution direct plasmonic comb spectroscopy with a high phase modulation index. The PDMS, which has an acoustic wave velocity six times lower than that of solid SiO_2, allows for a three to sixfold increase in the phase modulation index in the 0.1 ~2.0 MHz range. Easily moulded into various shapes, PDMS offers stable phase modulation with minimal effects from geometrical relations and external deformations. Even after 4,000 s of operation, the PDMS phase modulator shows no noticeable degradation or change of modulated frequencies. The frequency stability remained at approximately 2.48×10^{-18}, supporting that the PDMS phase modulator is suitable for long-term use. When coupled with plasmonic nanostructures, our μ-PDMS phase modulator demonstrates potential as a versatile spectroscopic tool. This modulator successfully generated FC modes spanning a 20 MHz frequency domain with 0.5 MHz spacing, achieving a spectral resolution 200 times higher. Leveraging this, we precisely measured the sub-MHz narrow linewidth of FPI in an absolute manner, referenced to the Rb atomic clock using the DFCS methodology. We provide a performance comparison of the state-of-the-art phase modulators to guide the tailored modulator for various applications (see Supplementary Note 4 for details). The PDMS phase modulator offers a compact and customizable design, making it compatible with various nanophotonic devices. This versatility highlights its potential for integration into photonic systems. Given its exceptional optical transparency from the visible to mid-infrared wavelength range and superior phase modulation capabilities, PDMS, when combined with plasmonic nanostructures, is expected to find applications in precision spectroscopy, coherent optical communications [45], precision laser ranging [46], and atomic & molecular clocks [33, 47, 48] in the future.

Methods

Evaluation of the phase modulation performances: phase modulation index and precision

For the comparative analysis of the phase modulation index between PDMS and SiO_2, all optical input powers emitted from the second harmonic generation of an erbium-doped fiber femtosecond laser source (C-Fiber high power, Menlo Systems) were kept constant. The second harmonic frequency comb (FC), injected into PDMS and SiO_2, has a beam diameter of about 500 μm. In these experiments, the dimensions of the PDMS sample followed the shape of the commercial SiO_2 sample, measuring 50 mm in width, 50 mm in length, and 10 mm in thickness. An acoustic wave was applied using a piezoelectric actuator (PA4GKH5 W, Thorlabs), controlled by a high-voltage amplifier (BP100, Thorlabs) and a multichannel waveform generator (DG4000, Rigol), which was referenced by the Rb atomic clock. The optical heterodyne beat was measured using a high-speed avalanche photodiode (APD210, Menlo Systems) paired with a high-resolution radio-frequency (RF) spectrum analyzer (E4440 A, Agilent). The phase modulation index was calculated from the total bandwidth of the modulation frequency using Carson's rule (see Supplementary Note 2).

Linewidth evaluation of phase-modulated FC

To evaluate the linewidth of the phase-modulated FC, we employed an external cavity diode laser (ECDL) (DL pro 780 nm, < 100 mW, Toptica) to generate an optical

heterodyne beat frequency with our phase-modulated FC (see Supplementary Fig. S2b). All laser sources were maintained in a transverse magnetic-field (TM) linear polarization state using half-wave plates and a linear polarizer. Unlike the experiments shown in Fig. 2, an additional acousto-optic frequency shifter is not required to observe the beat frequency, as the wavelength of the ECDL can be tuned directly.

Transmission spectrum measurement of Fabry-Pérot interferometer

For the μ-PDMS experiments, the FC was loosely focused using a plano-convex lens with a focal length of 125 mm and a beam diameter of 40 μm. The focused peak intensity on the plasmonic nanostructure was maintained at less than 0.1 MW cm^{-2} to minimize thermal damage to the sample. Fabry-Pérot interferometer (FPI) (SA30 - 73, Thorlabs) has a minimum finesse of 1500 and resolution of sub- 1 MHz. The phase-modulated FC propagates to the FPI which cavity length of the FPI was optimized at 50 mm to get a high-finesse by controlling a voltage of piezoelectric transducer. After passing through the FPI, the phase-modulated FC was coherently combined with a reference FC, resulting in the RF beat frequency. In the subsequent stage, a sawtooth waveform voltage was applied to actuate the piezoelectric transducer within the FPI to tune the cavity length. Consequently, the transmitted spectrum, directly correlated with the adjusted cavity length, was revealed by phase-modulated optical modes. These phase-modulated optical modes were subsequently encoded in the RF beat frequencies. To comprehensively profile the transmitted spectrum of the FPI in relation to shifts in the cavity length, we employed a continuous data capture approach to record snapshots of the RF beat results.

Preparation of PDMS for phase modulator

The PDMS sample was fabricated using a commercial kit (Sylgard 184, Sigma-Aldrich). The base and curing agent were mixed in a ratio of 10:1. Inner bubbles were degassed by placing the samples in a vacuum desiccator at − 0.06 MPa for 30 min. The mixture was then poured into a mold and cured on a hot plate at 70 °C for 2 h. The different types of piezoelectric actuator (PA4 FLW, PA3BCW, PA4 FKH3 W, Thorlabs) were affixed directly to the surface of the hardened PDMS. The fine air gap between the sample and the piezoelectric actuator was filled with ultrasound gel (Ultrasound Transmission Gel, Ecosonic).

Abbreviations

FC	Frequency comb
DFCS	Direct frequency comb spectroscopy
PDMS	Polydimethylsiloxane
FPI	Fabry-Pérot interferometer
μ-PDMS	Microscale-PDMS
AOM	Acousto-optic modulator
RF	Radio-frequency
SEM	Scanning electron microscope
SPP	Surface plasmon polariton
TM	Transverse magnetic-field
TE	Transverse electric-field
RBW	Resolution bandwidth
VBW	Video bandwidth
ECDL	External cavity diode laser
FWHM	Full width at half maximum

Supplementary Information

The online version contains supplementary material available at https://doi.org/10.1186/s43074-025-00170-x.

Supplementary Material 1

Acknowledgements
This work was supported by BrainLink program funded by the Ministry of Science and ICT through the National Research Foundation of Korea (RS- 2023 - 00236798) and BK21 FOUR Program by Pusan National University Research Grant, 2021. This work was supported by the National Research Foundation (NRF) grant funded by the Korean government (RS- 2024 - 00336583) and the Korea government (MSIT) (No. RS- 2024 - 00406152).

Authors'information
Reprints and permissions information is available at www.nature.com/reprints. Correspondence and requests for materials should be addressed to Y.-J. K. (yj.kim@kaist.ac.kr) and S. K. (s.kim@pusan.ac.kr).

Authors' contributions
The project was planned and overseen by Y. -J. K. and S. K.. PDMS phase modulator was prepared by San K.. Plasmonic Au nanohole array sample was prepared by San K. and T. -I. J.. All experiments were performed by San K.. Data were analyzed by San K., Y. -J. K., and S. K.. San K., R. A. T., K. K., Y. -J. K., and S. K. contributed to the manuscript preparation.

Funding
Not applicable.

Data availability
All data generated or analysed during this study are included in this published article [and its supplementary information files].

Declarations

Competing interests
The authors declare that they have no competing interests.

Received: 9 January 2025 Revised: 8 March 2025 Accepted: 1 April 2025
Published online: 14 April 2025

References

1. Spaun B, et al. Continuous probing of cold complex molecules with infrared frequency comb spectroscopy. Nature. 2016;533:517–20.
2. Changala PB, Weichman ML, Lee KF, Fermann ME, Ye J. Rovibrational quantum state resolution of the C60 fullerene. Science. 2019;363:49–54.
3. Dantus M, Bowman R, Zewail A. Femtosecond laser observations of molecular vibration and rotation. Nature. 1990;343:737–9.
4. Diddams SA, Hollberg L, Mbele V. Molecular fingerprinting with the resolved modes of a femtosecond laser frequency comb. Nature. 2007;445:627–30.
5. Hashimoto K, Badarla VR, Kawai A, Ideguchi T. Complementary vibrational spectroscopy. Nat Commun. 2019;10:4411.
6. Niering M, et al. Measurement of the hydrogen 1S–2S transition frequency by phase coherent comparison with a microwave cesium fountain clock. Phys Rev Lett. 2000;84:5496.
7. Ahmadi M, Alves B, Baker C, et al. Observation of the 1S–2S transition in trapped antihydrogen. Nature. 2017;541:506–10.
8. Grinin A, et al. Two-photon frequency comb spectroscopy of atomic hydrogen. Science. 2020;370:1061–6.
9. Mandon J, Guelachvili G, Picqué N. Fourier transform spectroscopy with a laser frequency comb. Nat Photonics. 2009;3:99–102.
10. Picqué N, Hänsch TW. Frequency comb spectroscopy. Nat Photonics. 2019;13:146–57.
11. Suh M-G, Yang Q-F, Yang KY, Yi X, Vahala KJ. Microresonator soliton dual-comb spectroscopy. Science. 2016;354:600–3.
12. Dutt A, et al. On-chip dual-comb source for spectroscopy. Sci Adv. 2018;4: e1701858.
13. Marin-Palomo P, Kemal J, Karpov M, et al. Microresonator-based solitons for massively parallel coherent optical communications. Nature. 2017;546:274–9.
14. Chang L, Liu S, Bowers JE. Integrated optical frequency comb technologies. Nat Photonics. 2022;16:95–108.
15. Hänsch TW. Nobel lecture: passion for precision. Rev Mod Phys. 2006;78:1297.
16. Eckstein JN, Ferguson A, Hänsch T. High-resolution two-photon spectroscopy with picosecond light pulses. Phys Rev Lett. 1978;40:847.
17. Marian A, Stowe MC, Lawall JR, Felinto D, Ye J. United time-frequency spectroscopy for dynamics and global structure. Science. 2004;306:2063–8.
18. Cingöz A, et al. Direct frequency comb spectroscopy in the extreme ultraviolet. Nature. 2012;482:68–71.
19. Canella A, et al. Low-repetition-rate optical frequency comb. Optica. 2024;11:1–9.

20. Ho K-P, Kahn JM. Optical frequency comb generator using phase modulation in amplified circulating loop. IEEE photon Technol Lett. 1993;5:721–5.
21. Saleh BEA, Teich MC. Chapter 20. In: Fundamentals of Photonics. 3rd ed. Hoboken: Wiley; 2019.
22. Wooten EL, et al. A review of lithium niobate modulators for fiber-optic communications systems. IEEE J Sel Top Quant Electron. 2000;6:69–82.
23. Snigirev V, Riedhauser A, Lihachev G, et al. Ultrafast tunable lasers using lithium niobate integrated photonics. Nature. 2023;615:411–7.
24. Li M, Ling J, He Y, et al. Lithium niobate photonic-crystal electro-optic modulator. Nat Commun. 2020;11:4123.
25. Zhang M, et al. Broadband electro-optic frequency comb generation in a lithium niobate microring resonator. Nature. 2019;568:373–7.
26. Rueda A, Sedlmeir F, Kumari M, Leuchs G, Schwefel HG. Resonant electro-optic frequency comb. Nature. 2019;568:378–81.
27. Hu Y, et al. High-efficiency and broadband on-chip electro-optic frequency comb generators. Nat Photonics. 2022;16:679–85.
28. Chang I. Acousto-optic devices and applications. Handb Opt. 1995;2(12):11-12.54.
29. Schrödel Y, Hartmann C, Zheng J, et al. Acousto-optic modulation of gigawatt-scale laser pulses in ambient air. Nat Photonics. 2024;18:54–9.
30. Kolle M, Lee S. Progress and opportunities in soft photonics and biologically inspired optics. Adv Mater. 2018;30:1702669.
31. Zhang X, Qiu J, Li X, Zhao J, Liu L. Complex refractive indices measurements of polymers in visible and near-infrared bands. Appl Opt. 2020;59:2337–44.
32. Wang Q, Han W, Wang Y, Lu M, Dong L. Tape nanolithography: a rapid and simple method for fabricating flexible, wearable nanophotonic devices. Microsyst Nanoeng. 2018;4:31.
33. Ludlow AD, Boyd MM, Ye J, Peik E, Schmidt PO. Optical atomic clocks. Rev Mod Phys. 2015;87:637.
34. Anh ND, et al. Plasmonic dynamics measured with frequency-comb-referenced phase spectroscopy. Nat Phys. 2019;15:132–7.
35. Bjorklund GC. Frequency-modulation spectroscopy: a new method for measuring weak absorptions and dispersions. Opt Lett. 1980;5:15–7.
36. Liu N, Cui Y, Khoo B, Zhang A. Damage characteristics of elastic material through a thin membrane using high-intensity focused ultrasound (HIFU). AIP Adv. 2018;8:115123.
37. Brick D, Emre E, Grossmann M, Dekorsy T, Hettich M. Picosecond photoacoustic metrology of SiO_2 and $LiNbO_3$ layer systems used for high frequency surface-acoustic-wave filters. Appl Sci. 2017;7:822.
38. Eschler H, Weidinger F. Acousto—optic properties of dense flint glasses. J Appl Phys. 1975;46:65–70.
39. Hong C, Yang S, Ndukaife JC. Stand-off trapping and manipulation of sub-10 nm objects and biomolecules using opto-thermo-electrohydrodynamic tweezers. Nat Nanotechnol. 2020;15:908–13.
40. Zhang Y, Min C, Dou X, et al. Plasmonic tweezers: for nanoscale optical trapping and beyond. Light Sci Appl. 2021;10:59.
41. Nguyen DA, Kim DH, Lee GH, et al. Real-time monitoring of fast gas dynamics with a single-molecule resolution by frequency-comb-referenced plasmonic phase spectroscopy. PhotoniX. 2024;5:22.
42. Geng X, Chun B, Seo J, et al. Frequency comb transferred by surface plasmon resonance. Nat Commun. 2016;7:10685.
43. Shih T-K, Chen C-F, Ho J-R, Chuang F-T. Fabrication of PDMS (polydimethylsiloxane) microlens and diffuser using replica molding. Microelectron Eng. 2006;83:2499–503.
44. Psaltis D, Quake S, Yang C. Developing optofluidic technology through the fusion of microfluidics and optics. Nature. 2006;442:381–6.
45. Li G. Recent advances in coherent optical communication. Optica. 2009;1:279–307.
46. Mitchell EW. Coherent laser ranging for precision imaging through flames. Optica. 2018;5:988–95.
47. Katori H. Optical lattice clocks and quantum metrology. Nat Photonics. 2011;5:203–10.
48. Kondov SS, et al. Molecular lattice clock with long vibrational coherence. Nat Phys. 2019;15:1118–22.

Publisher's Note